The role of the tip in non-contact atomic force microscopy dissipation images of ionic surfaces



2011 Nanotechnology 22 045702

(http://iopscience.iop.org/0957-4484/22/4/045702)

Nanotechnology **22** (2011) 045702 (9pp) doi:10.1088/0957-4484/22/4/045702

# The role of the tip in non-contact atomic force microscopy dissipation images of ionic surfaces

**F Federici Canova**[1] **and Adam S Foster**[1,2]

[1] Department of Physics, Tampere University of Technology, PO Box 692, FI-33010 Tampere, Finland
[2] Department of Applied Physics, Aalto University, PO Box 11100, FI-00076 Aalto, Finland

E-mail: filippo.federici@tut.fi

Received 20 August 2010, in final form 27 October 2010
Published 15 December 2010
Online at stacks.iop.org/Nano/22/045702

**Abstract**
In this paper we use simulations to investigate the role of the tip in nc-AFM measurements of dissipated energy. Using a virtual AFM we simulate the experiment focusing on the atomic scale energy dissipation on an NaCl(100) flat surface. The non-conservative interaction was treated with the theory of dynamic response and all the calculations were carried out using an atomistic model; several sets of tips were tested using ionic crystals (NaCl, KBr, MgO), each in different configurations (ideal, vacant, divacant, doped). Using an MgO-doped tip we were able to calculate a dissipation signal comparable to what is typically measured in experiments. It was not possible to see any dissipation with ideal tips, although they still have a significant interaction with the surface and give atomic contrast in the frequency shift signal. The effect of the scanning speed on measured frequency shift and dissipation is also calculated and discussed.

(Some figures in this article are in colour only in the electronic version)

## 1. Introduction

The non-contact atomic force microscope (nc-AFM) has proven to be an invaluable tool for imaging surfaces and molecules at the nanoscale [1]. A cantilever with an atomically sharp tip attached to its end is oscillated above the surface at its resonant frequency, subject to a harmonic potential [2]. As the tip approaches the surface, the atomic interactions between the two change the shape of the potential landscape and thus modify the resonant frequency of the cantilever, providing a direct measure of the tip–surface atomic interactions. In order to keep the oscillation amplitude at the setpoint value, an excitation signal drives the cantilever at the actual resonant frequency, compensating for its internal energy dissipation. As the cantilever scans the surface, the measured frequency shift can be used to deduce the interaction map or the topography of the surface with atomic resolution because the interaction potential is sensitive to the atomic species under the tip apex. The excitation amplitude required to balance the feedback also shows atomic scale variations and can be used to give a measurable atomic scale contrast on the surface [3]. This suggests that the internal dissipation is not the only mechanism taking energy away, demonstrating that there is an external dissipation process, happening at the atomic scale, that typically dissipates about 0.1–1 eV/cycle (but possibly higher [4, 5]). This dissipation or damping signal has been used to study a wide variety of different surfaces, including metals [6–8], semimetals [9–11], semiconductors [7, 12, 13], insulators [14–16] and insulating thin films [17–20]. Investigations have also targeted the influence of water layers [21], and molecules and molecular films [22–25] on the measured dissipation.

The damping signal developed as a focus for the scientific community because it often shows different features to frequency shift or topography maps, and offers insight into the coupling of the tip to phonon processes in the substrate. However, its interpretation still remains unclear, and there has been significant debate regarding the source of this damping signal, with several explanations formulated. Earlier works claimed the damping to be an artefact effect due to the non-ideal behaviour of the electronic components operating in an AFM [26, 27] and, consequently, of no physical interest. The stochastic friction mechanism [28–33] considers the energy dissipated by the induced friction from thermal

 

fluctuations of the tip and surface atoms, but it predicts dissipation orders of magnitude smaller than experimentally reported. Calculations of AFM energy dissipation on adsorbed overlayers were also carried out in [34], where nonlinear jumping of solitons in a bistable state is responsible for the hysteresis mechanism. The most accepted explanation suggests an adhesion hysteresis mechanism that makes the force on the tip different during approach and retraction. This is due to a reversible atomic reconstruction in the tip and/or surface at close approach [35–39] that decreases the oscillation amplitude and the feedback has to further compensate for the energy loss. The amplitude control response lag, as well as the phase mismatch between the oscillation and the driving excitation, induce small variations in the actual oscillation amplitude that give an apparent damping signal. Recent numerical simulations using this model within a virtual AFM simulator [40] produce a damping signal of the same order as experimentally reported [41], although direct comparison with experimental data for the same system has not been reported yet.

Tip–surface force hysteresis as a possible mechanism of dissipation has been seen in several other theoretical studies, including insulating [42], semiconducting [12, 43, 44] and metal surfaces [8]. Further support is given by molecular dynamics simulations on metallic systems [45], which show how an adhesion mechanism naturally occurs when a tip approaches the surface at low temperature. A key element in all these studies is the sensitivity of the measured dissipation to the specific atomic structure of the tip, and this is commonly seen in the wide variety of obtained experimental images for the same system [1] used in the experiment. A comprehensive study of the structure of large Si clusters as tips for imaging the silicon surface demonstrated that they exhibited a wide variety of metastable reconstructions that can be triggered by the interaction with the surface [43]. Depending on the tip model used, the dissipation was estimated in a quasi-static approach to be between 0.4 and 0.7 eV/cycle. This work established how the nature of the tip apex dominates the covalent interactions responsible for instabilities. In this paper we study in detail the role of the tip in nc-AFM energy dissipation on the ideal ionic NaCl(001) surface, a system class that has been prototypical in studies of dissipation [14, 15, 17, 24]. Starting from ideal ionic tips, but then gradually including the effects of defects and impurities we identify the conditions for reproducible damping contrast on an ideal surface. We demonstrate the importance of electrostatic interactions and polarization effects in this class of system. We will also show the influence of the response time of the circuits on dissipation images calculated with our virtual AFM program.

## 2. Methods

### *2.1. Virtual AFM*

Although AFM images can be calculated using simple analytical formulae [46–48] these methods neither include the effects of the full experimental apparatus nor non-conservative interactions. To capture those features we need to simulate the experiment with a virtual AFM [9, 41, 40, 49] that integrates the equation of motion of the cantilever subject to a static forcefield and a dissipative field using the Verlet velocity algorithm [50]; the static forcefield (see section 2.2) describes the short range interactions between the atoms in the tip and the surface, while the dissipative field (see section 2.3) provides the necessary information to compute the dynamic response of the surface atoms. A background van der Waals interaction is added to represent the interaction of the macroscopic part of the tip and the surface, given by an analytical formula [51] and depends only on the vertical position of the tip, its radius and material. In our case we set the tip radius to 10 nm, the cone angle to 30° and the Hamaker constant to $5.0 \times 10^{-19}$ N m, the value calculated for Si and NaCl [52]: the choice of these parameters does not affect the atomic features of the frequency shift, but only the overall value—hence the term background. The integration timestep was set to 10 ns to ensure a good enough numerical integration, and it is reduced to 0.1 ns as soon as the tip enters the dissipative field ($Z_{\text{tip}} < 8.0$ Å) to integrate the probability for the statistical jumps [36] correctly. The oscillation signal is processed by lowpass resistor–capacitor (RC) filters that output an amplitude signal. The signal is monitored as the value of the amplitude and is fed to the proportional–integral (PI) circuit in the automatic gain control (AGC) that tunes the excitation amplitude $R(t)$ in order to keep the amplitude itself constant. A clock measures the time delay between oscillation peaks to compute the frequency at every oscillation cycle; the results go through another set of lowpass filters and the frequency signal is recorded afterwards. The cantilever is driven by its own oscillation signal as in the self-excitation scheme, ensuring perfect phase match with the driving pulse; the excitation amplitude is regulated by the AGC, depending on the actual oscillation amplitude deviation from the setpoint.

The energy dissipation can be obtained from $R(t)$, the dynamic response of the AGC [2]:

$$E_{\text{D}} = \pi \frac{kA^2}{Q} \frac{R(t) - R(0)}{R(0)} \tag{1}$$

where $k$ is the cantilever's spring constant, $Q$ is its quality factor, $A$ is the amplitude and $R(0)$ is the feedback gain recorded with no tip–sample interaction. Since in the simulation we know exactly the normal force acting on the tip (it is the input for the simulation tool), we can directly integrate it along the oscillation path, providing a theoretical estimate for the dissipated energy. In all calculations the automatic distance control (ADC) was disabled, fixing the cantilever holder's height during each scan and the temperature for the dissipative process was set to 300 K. The temperature does not affect the virtual machine's components and there is no electronic or thermal noise superimposed on the evaluation of the forcefield [53]. Table 1 shows the parameters used to operate our virtual machine, where $f_0$, $k$ and $Q$ are the resonant frequency, spring constant and $Q$ factor of the cantilever, respectively, and $K_{\text{P}}^{\text{AGC}}$ and $K_{\text{I}}^{\text{AGC}}$ are the proportional and integral factors of the AGC feedback trying to keep the amplitude at the set point $A_0$. The parameters $f_{\text{cutoff}}^{\text{AGC}}$ and $f_{\text{cutoff}}^{\text{FD}}$ are the cutoff frequencies for the amplitude and

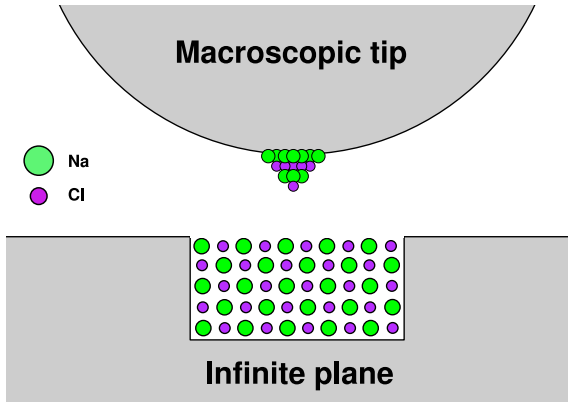


**Figure 1.** Snapshot of the model system used for calculation. The atomistic model captures only the termination of the tip and a small frame of the surface which are relevant for short range interactions. The macroscopic parts (grey areas) give the long range van der Waals background interaction.

frequency detector lowpass filters. The parameters regarding the cantilever correspond to typical values of real cantilevers used in nc-AFM experiments [1, 2, 48] and the other machine parameters are chosen to match a real apparatus. It has to be noted that, although the working principle of the virtual AFM is very similar to the one described in [40], we implemented our own simulation programme.

### 2.2. Static forcefield

The virtual AFM is a classical dynamics simulator, where there is only one particle (the tip) moving in a forcefield with some constraints (cantilever, ACG, etc). The forcefield has to be calculated beforehand and we obtain it through atomistic calculations of a model system including the tip termination and the surface. A model tip is placed at several points in the three-dimensional space above the surface, forming a volumetric data grid, where the forces acting on the tip are calculated. The data grid spans a surface area of $5.64 \times 5.64$ Å$^2$ and a vertical height of 20.0 Å and contains $8 \times 8 \times 200$ points. This is sufficient to describe the short range tip–surface interactions in the surface unit cell.

The macroscopic part of the tip is modelled as a cone with a round termination and the macroscopic surface is represented by an infinite plane (figure 1) and gives the background van der Waals interaction.

The calculations were performed using the SciFi code [54]. The interatomic forces are computed from a sum of pairwise Buckingham potentials acting between ions treated atomistically. Ions are treated within the shell model where each positively charged cores is coupled to its negative shell by a spring in order to describe the polarizability. Parameters for the species considered here were taken from [55–57]. Unless specified, all cores and shells were allowed to relax completely with respect to interatomic forces.

In our calculations we model the surface as a slab of NaCl consisting of 400 atoms arranged in four atomic layers. In experiments, the original silicon tip is usually oxidized by exposure to air or contaminated by contact with the surface, so the most likely tip terminations are one of the surface species or oxygen. Since the ion–ion interactions are fairly symmetric with respect to ionic charge, i.e. an Na-terminated tip interacting with Cl in the surface gives conservative interactions similar to a Cl-terminated tip interacting with Na in the surface, we focus mainly on negatively terminated tip models. Calculations with positively terminated tips show, as in previous studies [38], that this interaction symmetry is not present for dissipative interactions, so we also considered positive terminations where appropriate and the results are mentioned in the relevant sections.

**Table 1.** Parameters used to set up our virtual AFM.

| Parameter | Value |
|---|---|
| $f_0$ | 152 800.0 Hz |
| $k$ | 26 N m$^{-1}$ |
| $Q$ | 31 032 |
| $A_0$ | 30 nm |
| $K_{\mathrm{P}}^{\mathrm{AGC}}$ | 0.03 N m$^{-1}$ |
| $K_{\mathrm{I}}^{\mathrm{AGC}}$ | 0.45 N m$^{-1}$ s$^{-1}$ |
| $f_{\mathrm{cutoff}}^{\mathrm{AGC}}$ | 200 Hz |
| $f_{\mathrm{cutoff}}^{\mathrm{FD}}$ | 200 Hz |

Our basic models for an AFM tip consist of a 64-atom cube of NaCl, KBr or MgO [58], rotated in order to expose one vertex to the surface below, with three atomic layers on the top of the tip fixed to represent its macroscopic part (figure 2(a)). These tip models offer a balance between complete surface contamination (NaCl), an oxide-like tip (MgO) and a softer ionic model (KBr) [58–61]. We also investigated the possibilities of using more realistic $SiO_2$-based tip models, but they proved to be far too unstable with respect to surface atomic displacements within an atomistic model, and likely require a quantum treatment—prohibitive for detailed studies of dissipation at this point.

We start from these ideal tips to build other, more realistic tips, containing vacancies and impurities. The first set is obtained from the ideal one by removing one atom from the second atomic layer as schematically shown in figure 2(b). Since the second layer of our tips is formed from positive ions, the resulting tip will be negatively charged; we also considered tips with vacancies created in the middle of the structure, distant from the apex. The third set of tips was built by removing one atom in the second layer and one in the third layer of the ideal tip, making a divacant tip that is globally neutral, but has a strong structural defect close to the apex (figure 2(c)). The last set was built introducing a substitutional impurity in the middle of the tip so that the resulting tip is not neutral, but the excess charge is not located close to the apex (figure 2(d)). All these tips were fully relaxed to ensure stability before applying them to dissipation modelling.

### 2.3. Dissipative field

The static forcefield alone would not be able to give any dissipation, since there is no difference between the approach and retraction paths; for that, we need to describe how the

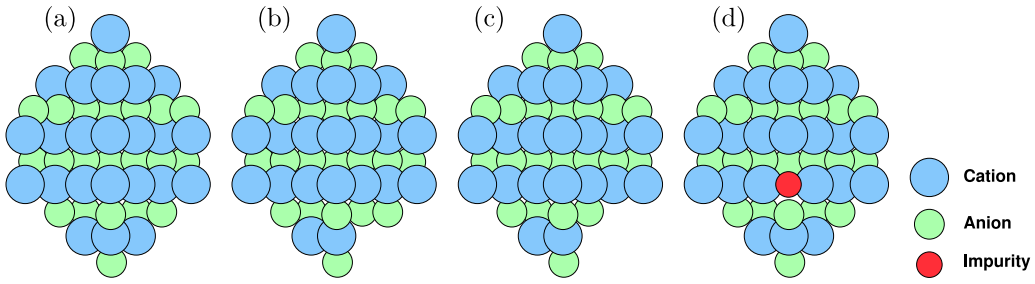


**Figure 2.** Schematic representation of ideal (a), vacant (b), divacant (c) and doped (d) tips: the white and blue circles represent negative and positive ions, respectively. The red circle represents the substitutional impurity, in this case a positive ion.

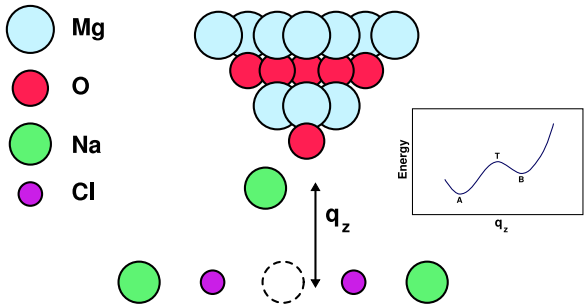


**Figure 3.** Schematic representation of the procedure (left) and typical energy curve (right) showing the two stable configurations A and B, and the transition state T.

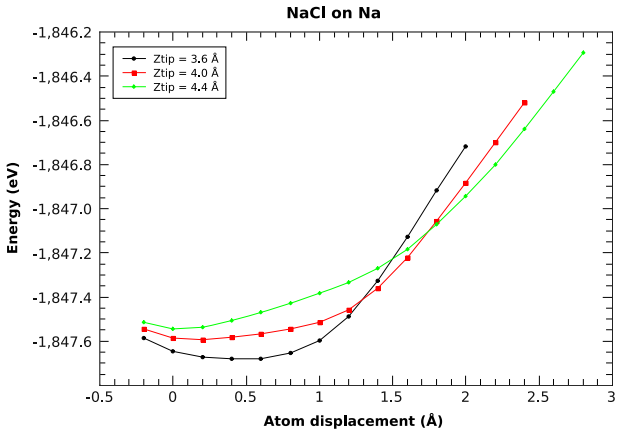


**Figure 4.** Energy curves calculated with an ideal NaCl tip above Na. The second state B does not arise.

adhesion mechanism works. According to the theory of dynamic response [36] the presence of the tip above the surface creates a secondary stable configuration for the system, obtained by displacing a surface atom from the ground state position towards the tip: the continuous hopping between the two stable states results in the adhesion mechanism responsible for energy dissipation. Once the stable configurations, namely A and B, and the transition state T in between have been identified, we can calculate the transition rates $W_{AB}$ and $W_{BA}$, as well as the forces acting on the tip in both cases, $F_A$ and $F_B$. The procedure is described in detail in [36] and summarized here.

We start with the tip at 8.0 Å above the surface and we identify the surface atom mostly affected by the tip—either though intuition or via running some molecular dynamics samples. Then we displace it gradually towards to tip and compute the energy at each step (figure 3). Only the vertical coordinate $q_z$ of the jumping atom is constrained and the atom is free to move within the $xy$ plane, and the rest of the system is allowed to relax. The tip is then gradually approached to the surface down to 3.0 Å distance and the bistable atom displacement procedure is repeated each time. The transition rates are given by

$$W_{AB} = \nu_A \exp\left(-\frac{E_{TA}}{k_B T}\right) \tag{2}$$

where $\nu_A$ is the attempt frequency calculated from the curvature of the minimum A, $E_{TA} = E_T - E_A$ is the energy barrier to overcome, $k_B$ the Boltzmann constant and $T$ the temperature. The reverse process transition rate $W_{BA}$ has an analogous expression. All this information builds a secondary data grid called dissipative field that will be used by the virtual machine to integrate the probability for the system to be in state A:

$$\frac{dP_A}{dt} = -P_A W_{AB} + P_B W_{BA} \tag{3}$$

where $P_B = 1 - P_A$. The transition rates depend on the position of the tip and the total tip–surface interaction becomes

$$\vec{F}(x, y, z) = P_A \vec{F}_A(x, y, z) + P_B \vec{F}_B(x, y, z) \tag{4}$$

## 3. Results

### *3.1. Ideal tips*

Ideal NaCl and KBr tips failed to produce the secondary state B. In figure 4 the energy curves obtained with an NaCl tip above a surface Na atom are shown. This situation occurs on all points on the surface, so the adhesion mechanism does not happen at all and there is no dissipated energy. The ideal MgO tip was able to generate the state B as shown in figure 5, although in a limited range of tip positions. As the tip oscillates above the surface, the second state is present only when $Z_{tip}$ is between 4.4 and 4.8 Å, and this region is not wide enough to allow the probability $P_A$ to smoothly evolve from 0 to 1 and back, and we computed a dissipated energy of the order

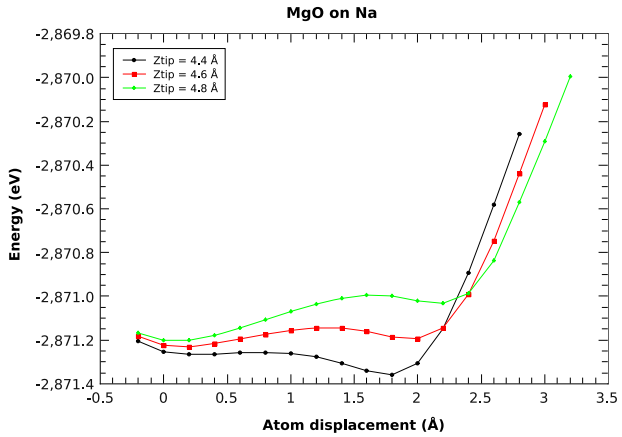


**Figure 5.** Energy curves calculated with an ideal MgO tip above Na. The second state B can be found only in a small range of $Z_{\text{tip}}$.

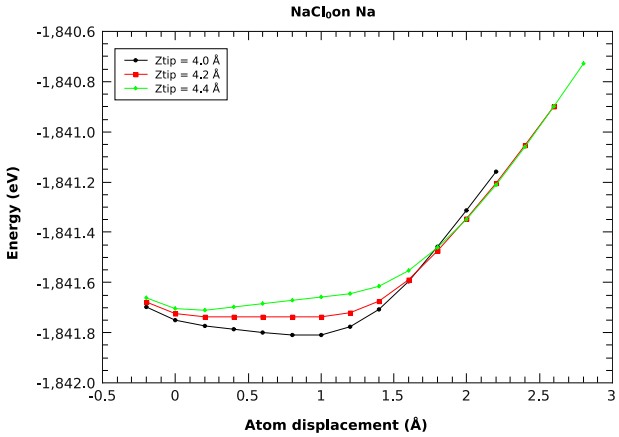


**Figure 6.** Energy curves calculated with an NaCl vacant tip above Na. Note that the second state B exists only for $Z_{\text{tip}} = 4.2$ Å.

of 0.1 meV/cycle—comparable to the order of the numerical noise.

The difference between NaCl (or KBr) and MgO ideal tips is due to the relative charges of ions in the different materials and the resultant charge on the apex. The net charge of oxygen is double that of chlorine/bromine and the MgO tip offers a more attractive termination to the surface Na atoms and they can find another stable position close to the tip. Note that, when using a positively terminated tip, for NaCl/KBr the different termination still results in no measurable dissipation. For MgO, using an Mg-terminated tip actually reduces the already very small predicted dissipation to below the measurable level.

### *3.2. Vacant tips*

Removing one atom close to the apex produced tips that were too unstable in our calculations. As the tip gets close to the surface major reconstructions occur in both tip and surface, and displacing one atom from the surface to compute the stable states caused further alterations that we cannot describe with our model. Creating the vacancy in the middle of the tip removes this problem, although results for NaCl (or KBr) and MgO tips are quite different. NaCl and KBr energy curves now have a second minimum, but in a very small range of tip heights (figure 6); thus the calculated energy dissipation is comparable to the numerical noise. The vacant MgO tip is now too reactive and the second state B is actually the global energy minimum (figure 7); as the tip approaches, the system flows from A to B and, upon retraction, it gets stuck there because the barrier $E_{\text{TB}}$ is too high, as shown in figure 7.

This means that an atom can be pulled away from the surface and attach to the tip, causing a tip-change event. This is a regular occurrence experimentally [17, 62–64], but within this modelling scheme leads to the formation of atomic chains, prohibiting site-dependent atomic dissipation processes [65].

### *3.3. Divacant tips*

The divacancy does not give any charge excess close to the apex, but provides a quite strong structural defect, making the

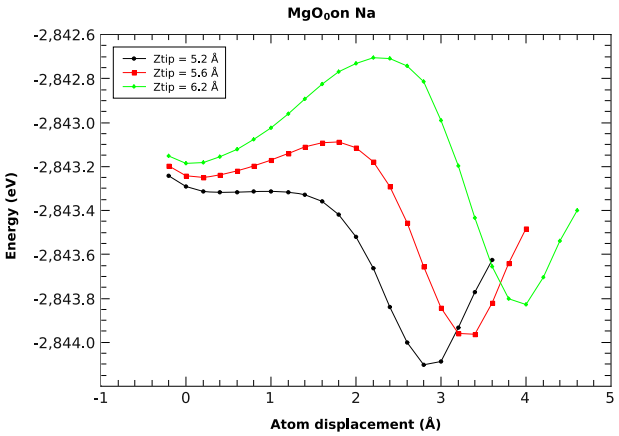


**Figure 7.** Energy curves calculated with an MgO vacant tip above Na. The state B is the ground state of the system.

tip termination softer. The energy curves for NaCl and KBr tips have a second minimum in a very small region (figure 8), and they behave like the tips with the vacancy in the middle of the structure. The same goes for the MgO divacant tip, showing the same behaviour as the vacant one (figure 9). The ground state of the system, on close approach, becomes B and as the tip retracts it becomes more stable until the system breaks down and the atom sticks to the tip. This time, the calculation was more troublesome to carry out, because the structural defect makes the apex prone to reconstruction: the O atom at the termination is likely to slide upwards and find a more stable configuration. In this configuration the tip gives no measurable dissipation signal.

### *3.4. Doped tips*

Starting from the ideal tips, we changed one atom in the inner part of the structure in order to enhance the Coulomb interaction between the tip and the surface. In the case of NaCl and KBr tips, one Cl (or Br) atom was replaced with oxygen, giving the tip a net charge of $-1e$. This is still not enough to produce the second state in the energy curves in a reasonable range of tip heights and we cannot operate the

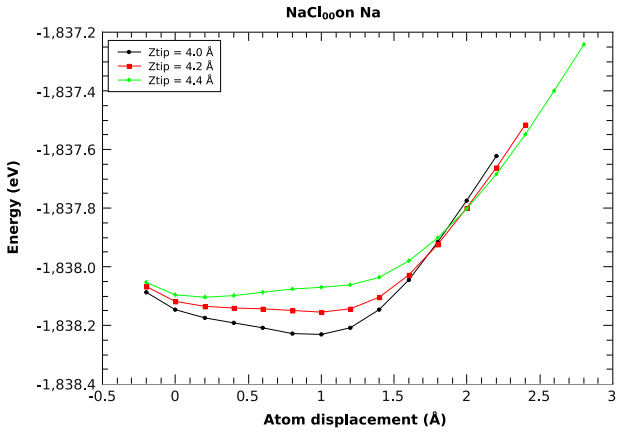


**Figure 8.** Energy curves calculated with an NaCl vacant tip above Na. Note that the second state B exists only for $Z_{\text{tip}} = 4.2$ Å.

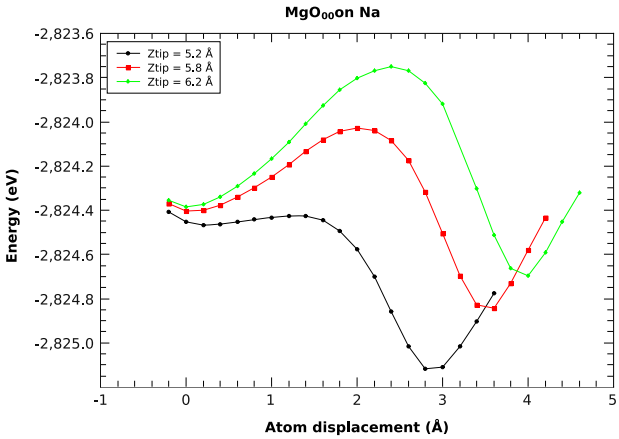


**Figure 9.** Energy curves calculated with an MgO divacant tip above Na. The second state B is the ground state of the system.

virtual machine with these tips. Replacing an Mg atom with Na in the middle of an MgO tip produced a doped tip with the desired characteristics: on approach the system does not show complex or irreversible reconstruction and both the minima A and B could be found in a significant range of tip heights. Using the forcefield and the dissipative field calculated with this tip we could simulate an nc-AFM experiment and obtain an energy dissipation of about 0.1 eV/cycle. In figure 10 we can see the dependence on the tip's maximum approach of the dissipated energy measured above Na and Cl atoms. The virtual AFM is operated in the steady state, i.e. each point in the curves is the dissipation value recorded after the cantilever was oscillating for 0.5 s on the same spot. This way the AGC has time to adjust and the oscillation amplitude recovers the setpoint value within 0.1 pm deviation. At close approach both Na and Cl appear to dissipate energy, but as the tip oscillates further, the dissipation on chlorine rapidly fades to zero, while on sodium it can be observed up to 5.6 Å—as expected for a negatively terminated tip, with a net negative charge. The same steady state measurement technique, applied to all the other points on the surface, allows us to build images of the dissipated energy: figure 11 shows two dissipation maps at closest approach distances of 4.5 and

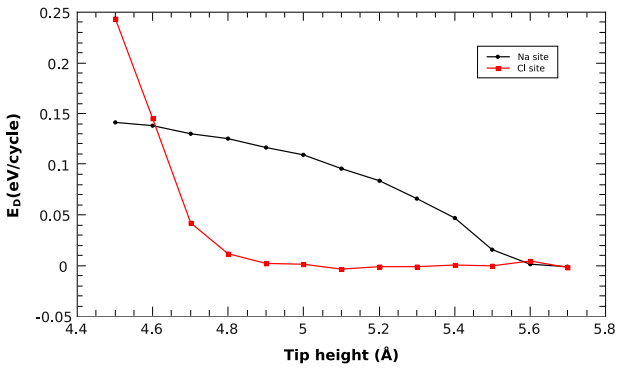


**Figure 10.** Energy dissipation calculated with a virtual AFM in the steady state above Na atom (black circles) and Cl atom (red squares).

5.5 Å. The image scanned at 4.5 Å (figure 11(b)) shows no atomic pattern and the dissipation is high for all the points on the surface. As the tip probes at higher distances (figure 11(a)), the dissipation around Cl vanishes and the atomic structure of the surface becomes visible. The steady state regime allows us to see the actual energy dissipation without influence from the non-ideal behaviour of the feedback gain: this is confirmed by the fact that the dissipation measured from the feedback signal and the one computed integrating the tip–sample force over the tip's trajectory are the same within 1%. Comparing these results with images scanned at finite speed allows us to identify any possible artefact effects due to the instrumentation. Figure 12 shows a comparison between the image scanned with the dissipative field disabled ((a) and (b)) and enabled ((c) and (d)). The damping signal obtained excluding the non-conservative interaction does not have any atomic scale features, confirming previous studies [41]. Furthermore, we point out how the inclusion of a non-conservative field alters the frequency shift signal that is usually associated with purely conservative forces. The finite scan speed produces an apparent drift in the shape of the bright spots that looked circular in the steady state image: this is induced by the response time of the feedback loop. Images calculated at a scan speed of 5.0 nm s$^{-1}$ (figure 13) show how this feature is enhanced at higher speeds. Comparing the frequency shift maps scanned at 1 nm s$^{-1}$ (figure 12(d)) and at 5 nm s$^{-1}$ (figure 13(b)) an apparent contrast inversion occurs. At higher speed the feedback response lag causes the amplitude to differ from the setpoint value and the frequency shift seems to be mostly affected, although the damping signal is not. The robustness of the dissipation signal to increased scanning speeds was also seen to a lesser extent in studies of the CaO surface [41], although it required speeds of 100 nm s$^{-1}$ to observe it.

Note that the ring shape of the bright spots in figure 11(a) is a consequence of the unstable behaviour of the system. At first sight, it could be argued that the distance between the dark and bright parts in the ring is 0.705 Å, which corresponds to the spacing between the grid points where all the quantities are calculated. The energy barriers are calculated exactly only in those grid points and interpolated in the middle; it happens that the calculation done on the Na sites is stable in a smaller

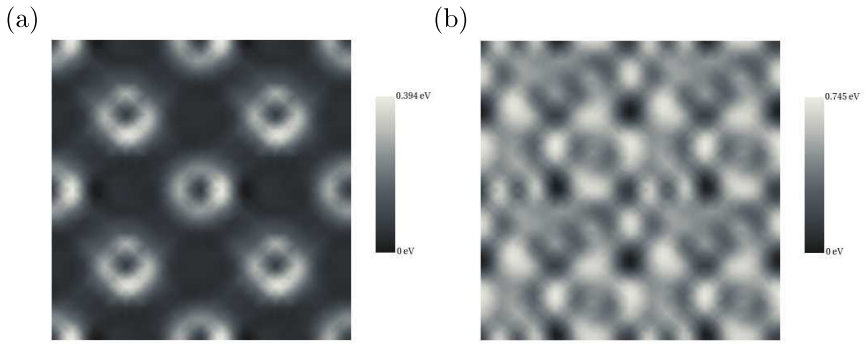


**Figure 11.** Energy dissipation maps obtained from the steady state calculations at far (a) and close (b) approach. The image area is $8.46 \times 8.46$ Å$^2$. (a) $Z_{\text{tip}} = 5.5$ Åand (b) $Z_{\text{tip}} = 4.5$ Å.

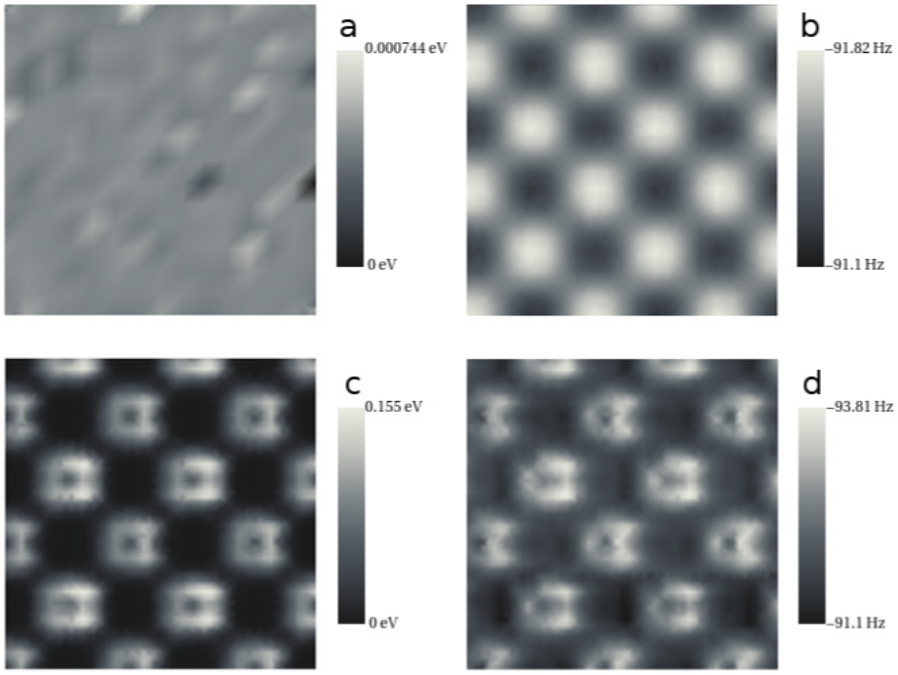


**Figure 12.** Damping signal ((a), (c)) and frequency shift maps ((b), (d)). The top images ((a), (b)) were obtained using the conservative forcefield only; for the bottom ones ((b), (d)) the non-conservative interaction was also enabled. The scans were performed at a speed of 1.0 nm s$^{-1}$ at 5.5 Å height over an area of $1.41 \times 1.41$ nm$^2$.

range of tip heights ($Z_{\text{tip}} \leqslant 6.0$ Å), because the tip–surface interaction reaches its maximum and the energy curves are not well behaved. For the adjacent grid points, the interaction is weaker and the energy curves are stable for higher tip positions ($Z_{\text{tip}} \leqslant 6.8$ Å). This way the statistical reconstruction can occur in a smaller range of the tip oscillation cycle above Na than the near positions, thus reducing the amplitude of the force hysteresis loops and decreasing the dissipation. The dark spot in the centre of the bright bump is thus caused by a computational artefact. Sampling a finer grid around Na atoms proved that the process is actually unstable only within 0.2 Å around Na, meaning that the dark spot in the ring should be much smaller than how it currently appears, but performing the whole calculation on such a fine grid is computationally too expensive. A similar ring structure was seen in earlier simulations of dissipation on the CaO(001) surface [38].

## 4. Discussion

Our calculations confirm the strong dependence on the tip of the nc-AFM energy dissipation seen experimentally and predicted for other surfaces in simulations. Out of the large number of tip models considered in the study, only one predicted measurable dissipation on the ideal NaCl(001) surface. Undefected nanocluster tips are too stable, preventing any significant atomic reconstruction in the non-contact regime. On the other hand, our first attempts to make the tip more reactive (by creating apex vacancies and divacancies)

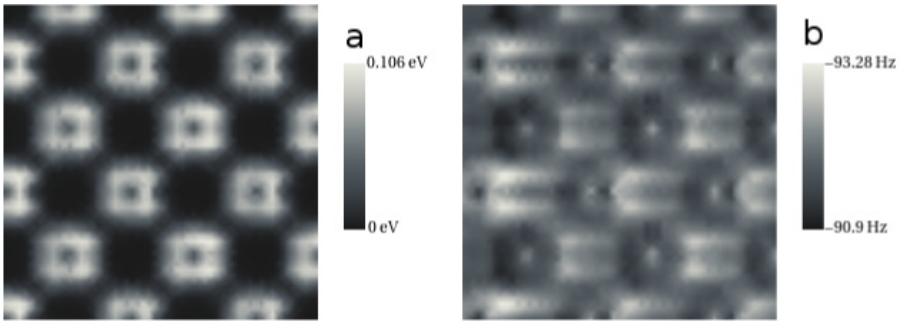


**Figure 13.** Damping signal (a) and frequency shift maps (b) calculated at a scan speed of 5.0 nm $s^{-1}$ at 5.5 Å height. The image area is $1.41 \times 1.41$ $nm^2$.

were unsuccessful as the system became too unstable, leading to either a permanent tip change or a reaction path that could not be described by a single atomic coordinate. Doping an MgO tip maintains the stability necessary to avoid tip changes, but adds a longer range electrostatic charge/dipole interaction. This extends the range of reversible induced surface atom displacements and hence increases the hysteresis and predicted dissipation. The resultant dissipated energy per cycle and the obtained damping contrast are in reasonable agreement with experimental measurements on the same or similar systems. Note that a doped oxide tip is a reasonable model for the kind of contaminated silica tips expected in experiments. This is an important step in defining the properties of tips that result in measurable dissipation in ionic systems, while re-emphasizing that dissipation in these systems is not an artefact of the experimental set-up.

An interesting result of our speed-dependent calculations is the demonstration that the damping signal is less affected by the feedback response time than the frequency shift. This is a further consequence of the signal being more sensitive to the atomic processes occurring at the tip apex, but suggests dissipative tips would allow atomic resolution in the damping contrast at much higher speeds than conventionally used. The dissipation maps calculated from the damping signal are very similar to the ones estimated by integrating the force along the oscillation path, exhibiting the same features and they match to within 0.01 eV/cycle, proving that the approximations used to deduce the dissipation from the excitation amplitude work nicely.

Although the computational demands of a full dissipation simulation are very restrictive on the tip–surface interaction scheme that can be used, it is important to evaluate the approximations implemented with respect to the kind of atomic processes we are modelling. In general, the atomistic potentials used in the calculations were designed to reproduce the bulk and surface properties of ionic crystals and are fitted to the equilibrium state. Induced tip and surface atomic displacements are inherently non-equilibrium processes, outside the scope of the original potential design. Comparisons to first-principles displacement profiles for ideal and doped NaCl show that the potentials perform remarkably well for displacements of up 0.05 nm [66], but beyond this the potentials cannot capture the electron transfer processes that can occur. This results in an overemphasis on the ionicity of the system by the model in all processes, and atomic jumps occur more frequently and at longer range [65] than would be expected with a quantum framework. The direct result for this work is that some tips we neglected due to instability may be stable within a more accurate interaction scheme. This problem is further enhanced by the zero-temperature approximation used when calculating the tip–surface interactions (note that finite temperature is included when calculating the dissipation from the non-conservative field). At finite temperature, it is likely that several of the predicted tip-change events would be more reversible, again reducing the set of discarded tip models, although we may also observe new tip-change events. More generally, the assumption of purely ionic tip models is certainly a significant approximation and matches experiment only when the tip apex has been heavily contaminated by the surface or has picked up a nanocluster. Certainly, including some elements of the original silicon/silica tip, or even functionalized tips [67], in some of the tip models would be desirable—however, our initial studies in this direction demonstrate that existing interaction models are not suitable and would require significant re-design.

Again we emphasize that going beyond this classical approach for full dissipation simulations requires significant methodological developments and can be considered a work in progress. Further studies, applying dissipative tips to more complex surfaces and also including steps, defects and adsorbates should aid in providing a more systematic understanding of high resolution dissipation images. Alongside simulations of other classes of tip and the inclusion of finite temperature at all levels, this will provide an important framework for reliable integration of dissipation measurements into the AFM toolbox.

## Acknowledgments

We would like to thank the European Science Foundation through the FANAS programme and the Finnish Academy of Science and Letters, Vilho, Yrjö and Kalle Väisälä Foundation for financial support. We are grateful to Lev Kantorovich for useful discussion and critical reading of the manuscript.

## References


[1] Morita S, Weisendanger R and Meyer E 2002 *Non-Contact Atomic Force Microscopy* (Berlin: Springer)
[2] Giessibl J 2003 *Rev. Mod. Phys.* **75** 957
[3] Anczykowski B, Gotsmann B, Fuchs H, Cleveland J P and Elings V B 1999 How to measure energy dissipation in dynamic mode atomic force microscopy *Appl. Surf. Sci.* **140** 376–82
[4] Giessibl F J, Herz M and Mannhart J 2002 Friction traced to the single atom *Proc. Natl Acad. Sci. USA* **99** 16010
[5] Martinez N F and Garcia R 2006 *Nanotechnology* **17** S167
[6] Pfeiffer O, Nony L, Bennewitz R, Baratoff A and Meyer E 2004 *Nanotechnology* **15** S101–7
[7] Ozer H O, O'Brien S J, Norris A, Sader J E and Pethica J B 2005 *Japan. J. Appl. Phys.* **44** 5325–7
[8] Caciuc V, Hoelscher H, Weiner D, Fuchs H and Schirmeisen A 2008 *Phys. Rev.* B **77** 045411
[9] Couturier G, Aime J P, Salardenne J, Boisgard R, Gourdon A and Gauthier S 2001 *Appl. Phys.* A **72** S47–50
[10] Hembacher S, Giessibl F J and Mannhart J 2005 *Phys. Rev. Lett.* **94** 056101
[11] Filleter T, McChesney J, Bostwick A and Rotenberg E 2009 *Phys. Rev. Lett.* **102** 086102
[12] Oyabu N, Pou P, Sugimoto Y, Jelinek P, Abe M, Morita S, Pérez R and Custance O 2006 *Phys. Rev. Lett.* **96** 106101
[13] Ozer H O, Atabak M and Oral A 2003 *Appl. Surf. Sci.* **210** 12–7
[14] Maier S, Pfeiffer O, Glatzel T, Meyer E, Filleter T and Bennewitz R 2007 *Phys. Rev.* B **75** 195408
[15] Bennewitz R, Schär S, Gnecco E, Pfeiffer O, Bammerlin M and Meyer E 2004 *Appl. Phys.* A **78** 837
[16] Torbrügge S, Reichling M, Ishiyama A, Morita S and Custance O 2007 *Phys. Rev. Lett.* **99** 056101
[17] Bennewitz R, Foster A S, Kantorovich L N, Bammerlin M, Loppaher C, Schär S, Guggusberg M, Meyer E and Shluger A L 2000 *Phys. Rev.* B **62** 2074
[18] Seino Y, Yoshikawa S, Abe M and Morita S 2007 *J. Phys.: Condens. Matter* **19** 445001
[19] Loppacher C, Bennewitz R, Pfeiffer O, Guggisberg M, Bammerlin M, Schär S, Barwich V, Baratoff A and Meyer E 2000 *Phys. Rev.* B **62** 13674–9
[20] Hoffmann R, Baratoff A, Hug H J, Hidber H R, v Löhneysen H and Güntherodt H J 2007 *Nanotechnology* **18** 395503
[21] Nony L, Cohen-Bouhacina T and Aim J P 2002 *Surf. Sci.* **499** 152–60
[22] Fukuma T, Umeda K, Kobayashi K, Yamada H and Matsushige K 2002 *Japan. J. Appl. Phys.* **41** 4903
[23] Fukuma T, Ichii T, Kobayashi K, Yamada H and Matsushige K 2004 *J. Appl. Phys.* **95** 1222–6
[24] Nony L, Bennewitz R, Pfeiffer O, Gnecco E, Baratoff A, Meyer E, Eguchi T, Gourdon A and Joachim C 2004 *Nanotechnology* **15** S91–6
[25] Roll T, Kunstmann T, Fendrich M, Moeller R and Schleberger M 2008 *Nanotechnology* **19** 045703
[26] Gauthier M, Pérez R, Arai T, Tomitori M and Tsukada M 2002 *Phys. Rev. Lett.* **89** 146104
[27] Gauthier M and Tsukada M 2000 *Phys. Rev. Lett.* **85** 5348
[28] Gauthier M and Tsukada M 1999 *Phys. Rev.* B **60** 11716
[29] Mo M Y and Kantorovich L 2001 *J. Phys.: Condens. Matter* **13** 1439–59
[30] Kantorovich L N 2001 *J. Phys.: Condens. Matter* **13** 945–58
[31] Kantorovich L N 2001 *Phys. Rev.* B **64** 245409
[32] Kantorovich L N 2002 *J. Phys.: Condens. Matter* **14** 4329–43
[33] Kantorovich L N 2002 *Surf. Sci.* **521** 117–28
[34] Negri C, Manini N, Vanossi A, Santoro G E and Tosatti E 2010 *Phys. Rev.* B **81** 045417
[35] Hoffmann P M, Jeffery S, Pethica J B, Özer H O and Oral A 2001 *Phys. Rev. Lett.* **87** 265502
[36] Kantorovich L and Trevethan T 2004 *Phys. Rev. Lett.* **93** 236102
[37] Trevethan T and Kantorovich L 2005 *Nanotechnology* **16** S79
[38] Trevethan T and Kantorovich L 2006 *Nanotechnology* **17** S205
[39] Sasaki N and Tsukada M 2000 *Japan. J. Appl. Phys.* **39** L1334
[40] Polesel-Maris J and Gauthier S 2005 *J. Appl. Phys.* **97** 044902
[41] Trevethan T, Kantorovich L, Polesel-Maris J and Gauthier S 2007 *Nanotechnology* **18** 084017
[42] Watkins M, Trevethan T, Shluger A L and Kantorovich L 2007 *Phys. Rev.* B **76** 245421
[43] Ghasemi S A, Goedecker S, Baratoff A, Lenosky T, Meyer E and Hug H J 2008 *Phys. Rev. Lett.* **100** 236106
[44] Dieska P, Stich I and Pérez R 2005 *Phys. Rev. Lett.* **95** 126103
[45] Pishkenari H N and Meghdari A 2010 *Physica* E **42** 2069
[46] Giessibl F J 1997 *Phys. Rev.* B **56** 16010
[47] Livshits A I, Shluger A L, Rohl A L and Foster A S 1999 *Phys. Rev.* B **59** 2436
[48] García R and Pérez R 2002 *Surf. Sci. Rep.* **47** 197
[49] Couturier G, Aimé J, Salardenne J and Boisgard R 2001 *Eur. Phys. J.* AP **15** 141–7
[50] Allen M P and Tildesley D J 2002 *Computer Simulation of Liquids* (Oxford: Clarendon)
[51] Argento C and French R H 1996 *J. Appl. Phys.* **80** 6081
[52] French R H, Cannon R M, Denoyer L K and Chiang Y M 1995 *Solid State Ion.* **75** 13–33
[53] Polesel-Maris J, de la Cerda M A V, Martrou D and Gauthier S 2009 *Phys. Rev.* B **79** 235401
[54] Kantorovich L, Foster A S, Shluger A L and Stoneham A M 2000 *Surf. Sci.* **445** 283
[55] Sangster M J L and Atwood R M 1978 *J. Phys. C: Solid State Phys.* **11** 1541
[56] Grimes R, Catlow C and Stoneham A 1989 *J. Phys.: Condens. Matter* **1** 7367
[57] Shluger A L, Rohl A L, Gay D H and Williams R T 1994 *J. Phys.: Condens. Matter* **6** 1825
[58] Hofer W A, Foster A S and Shluger A L 2003 *Rev. Mod. Phys.* **75** 1287
[59] Sushko P V, Foster A S, Kantorovich L N and Shluger A L 1999 *Appl. Surf. Sci.* **144–145** 608–12
[60] Barth C, Hynninen T, Bieletzki M, Henry C R, Foster A S, Esch F and Heiz U 2010 *New J. Phys.* **12** 093024
[61] Bieletzki M, Hynninen T, Soini T M, Pivetta M, Henry C R, Foster A S, Esch F, Barth C and Heiz U 2010 *Phys. Chem. Chem. Phys.* **12** 3203–9
[62] Enevoldsen G H, Foster A S, Christensen M C, Lauritsen J V and Besenbacher F 2007 *Phys. Rev.* B **76** 205415
[63] de la Cerda M A V, Abad J, Madgavkar A, Martrou D and Gauthier S 2008 *Nanotechnology* **19** 045503
[64] Gritschneder S and Reichling M 2008 *J. Phys. Chem.* C **112** 2045
[65] Lantz M A, Hoffmann R, Foster A S, Baratoff A, Hug H J, Hidber H R and Güntherodt H J 2006 *Phys. Rev.* B **74** 245426
[66] Foster A S, Barth C and Henry C R 2009 *Phys. Rev. Lett.* **102** 256103
[67] Gross L, Mohn F, Moll N, Liljeroth P and Meyer G 2009 *Science* **325** 1110–4